Electrical manipulation of oligonucleotides grafted to charged surfaces†

Ulrich Rant,*[a] Kenji Arinaga,[a,b] Shozo Fujita,[b] Naoki Yokoyama,[b] Gerhard Abstreiter[a] and Marc Tornow[a]

Received 21st April 2006, Accepted 10th July 2006
First published as an Advance Article on the web 17th August 2006
DOI: 10.1039/b605712h

The electrical manipulation of short DNA molecules on surfaces offers novel functionalities with fascinating possibilities in the field of bio-interfaces. Here we present systematic investigations of the electrical interactions which govern the structure of oligonucleotides on charged gold surfaces. Successively, we address influences of the applied field strength, the role of DC electrode potentials, in particular for polycrystalline surfaces, as well as screening effects of the surrounding electrolyte solution. Data obtained for single and double stranded DNA exhibit differences which can be attributed to the dissimilar flexibility of the different molecular conformations. A comparison of the experimental results with a basic model shows how the alignment of the molecules adjusts according to a balance between electrically induced ordering and stochastic thermal motions. The presented conclusions are expected to be of general relevance for the behaviour of polyelectrolytes exposed to localized electric fields at interfaces.

Introduction

A central element of many future bio-engineered nano-devices will be the interface between a bio-nano building block and a macroscopic unit. Chemically grafted oligonucleotides on surfaces may constitute such an interface by linking a DNA-based nanostructure to a solid support. To date, DNA monolayers have already found importance applications, for instance as sensing probes[1] in DNA microarrays.[2] During the recent past, considerable effort has been made to characterize the complex adsorption mechanisms of nucleic acids on surfaces,[3–5] mainly focusing on chemical aspects of the DNA surface interactions.

In prospect of a higher sophistication in these bio-layers, it is desirable to actively manipulate the layer structure, because this can significantly enhance their functionality and provide the basis for new device concepts. Owing to the strong intrinsic negative charge of DNA, electric fields are efficient and convenient means to do so, as was shown for the first time by Kelley *et al.*[6] who induced a change in the orientation of a DNA layer by altering the potential of the substrate which supported the layer. Recently, truly 'switchable' DNA layers have been realized and it was demonstrated that the conformation of DNA layers can be modulated even at high frequencies with outstanding persistency.[7,8] The influence of the substrate potential on the alignment and ordering of nucleic acids on surfaces has also been recognized in the context of scanning probe microscopy experiments,[9,10] including measurements addressing the electrical conductance of DNA.[11]

In this article we present systematic studies addressing the response of surface-tethered oligonucleotides on gold surfaces to variations in the electrode potential. Examining the behaviour of nucleic acids on charged metal surfaces which are in contact with electrolyte solution is particularly intriguing since the metal/liquid interface constitutes a highly polarized region:[12] the electric field decays quasi-exponentially into solution on length scales of typically a few nm, which corresponds to a fraction of the contour length of oligonucleotides (the nucleic acids used in this study are 8 or 16 nm long, respectively). Thus, the DNA is located within an pronounced electric field gradient and, at the same time, exposed to high field strengths (up to 10^7 V cm^{-1}) even for moderate electrode potentials of only a few hundred mV (which is a 'harmless' electrochemical regime).

The paper is structured as follows: after introducing the sample preparation and elucidating the fluorescence quenching techniques used to assess the average DNA layer height, we focus on three aspects. These are (i) the magnitude of the applied electric field, (ii) the role of DC bias and the potential of zero charge, and (iii) electrostatic screening effects originating from the surrounding salt solution. We present experimental data obtained for single (*ss*) and double stranded (*ds*) nucleic acids as well as two distinct oligonucleotide lengths, namely 24 and 48 base pairs (bp), respectively. We find intriguing differences in the behaviour of *ss* and *ds*-DNA which can be attributed to their dissimilar molecular flexibilities. The results are discussed within the Gouy–Chapman–Stern (GCS) theory of polarized solid/electrolyte interfaces and compared to a simple model which describes the average orientation of DNA in the external field as a balance between electrically induced ordering and thermally induced disordering of the layer structure. Our findings are expected to be generally applicable to the behaviour of polyelectrolytes on charged substrates.

Materials and methods

Self-assembled layers of single stranded oligonucleotides of a mixed, non self-complementary sequence were prepared on gold surfaces by adsorption from aqueous solution.

Gold electrodes of 2.0 mm diameter were prepared on 3 inch single crystalline sapphire wafers by subsequently depositing thin

[a]*Walter Schottky Institute, Technical University Munich, Am Coulombwall 3, 85748, Garching, Germany. E-mail: rant@wsi.tum.de.; Fax: +49 89 320 6620; Tel: +49 89 289 12770*
[b]*Fujitsu Laboratories, Atsugi, 243–0197, Japan*
† This paper was published as part of a themed issue on DNA-Based Nano-Architectures and Nano-Machines.

layers of Ti (10 nm), Pt (40 nm), and Au (200 nm) using standard optical lithography and metallization techniques. The Ti layer promotes adhesion between the Au film and the substrate while the Pt interlayer constitutes a precautionary measure to prevent potential diffusion between Ti and Au when cleaning the electrodes in hot solutions. Prior to DNA adsorption, the electrodes were cleaned in Piranha solution (H_2SO_4 : H_2O_2(30%) = 7 : 3) and exposed to HNO_3 (60%) for 15 min each, followed by a final rinse with deionized water. The roughness of the gold surface was measured by atomic force microscopy yielding RMS values of approximately 1 nm; hence, roughness influences can be neglected on the length scale of the used oligonucleotides.

Oligonucleotides were obtained from IBA GmbH, Goettingen, Germany. The sequences of the 24 mer and 48 mer oligonucleotides were 5′ HS-$(CH_2)_6$–TAG TCG TAA GCT GAT ATG GCT GAT–Cy3 3′ and 5′ HS-$(CH_2)_6$–TAG TCG TAA GCT GAT ATG GCT GAT TAG TCG GAA GCA TCG AAC GCT GAT–Cy3 3′, respectively. The 5′ ends were modified with a thiol linker in order to graft the strands chemically to the surface (S–Au bond). Single stranded oligonucleotides were adsorbed onto the surface by exposing the Au electrodes to Tris-buffered electrolyte solution of low salinity ([Tris] = 10 mM, pH = 7.3) containing 1 μM DNA for 5 min. Afterwards, the samples were thoroughly rinsed with buffer solution ([Tris] = 10 mM, [NaCl] = 50 mM, pH = 7.3). Subsequently, a second adsorption step was carried out, during which a monolayer of short spacer molecules, mercaptohexanol (MCH, obtained from Sigma Aldrich), was co-adsorbed on the DNA modified surface ([MCH] = 1 mM, [Tris] = 10 mM, [NaCl] = 50 mM, pH = 7.3, incubation time ~1 h). By forming a dense sub-layer, MCH aids prevention of non-specific interactions between DNA and the gold surface.[13] After rinsing the samples again they were finally kept in Tris-buffer ([Tris] = 10 mM, pH = 7.3), which was also used during the measurements.

The adsorption process had previously been optimized to yield DNA layers of low surface coverage,[14] in order to prevent steric interactions between neighbouring strands,[7] which would significantly affect the efficiency of the electrical manipulation. The surface coverage was determined using electrochemical methods,[15] yielding 1.7×10^{11} and 2.6×10^{11} molecules cm^{-2} for the 48 mer and 24 mer samples, respectively, which are shown in Figs. 1, 2, and 4; a coverage of 3.3×10^{11} molecules cm^{-2} was determined for the sample shown in Fig. 5. The error of the coverage quantification is estimated from the minimal DNA surface density for which the electrochemical response from the DNA-bound ruthenium-hexaamine marker is distinguishable from the background noise, and was approximately 5×10^{10} molecules cm^{-2}.

After having performed measurements in its single stranded conformation, the layers were hybridized with nucleic acids of complementary sequence ([cDNA] = 1 μM) in 200 mM NaCl solution. The measurements were then repeated with the same layers in their double stranded conformation. The hybridization efficiency for low-density *ss*-DNA layers as used here is expected to be nearly 100%, as indicated by, for instance, Herne *et al.*[13] and our own experience from measuring the molecule density on the surface before and after hybridization by electrochemical means.

Electrical potentials were applied to the Au substrates *vs.* a Ag/AgCl reference electrode using a commercially available potentiostat system (Autolab, Ecochemie, The Netherlands) and a Pt counter electrode.

The upper (3′) ends of the oligonucleotides were dye-labeled with a fluorescence marker (Cy3™) for optical detection. An argon ion laser (515 nm) was used as excitation light source. The emitted fluorescence light was collected by an optical fiber, passed through a 0.5 m monochromator (Jobin Yvon, France), set to the Cy3 peak emission wavelength (565 nm), and detected by a cooled photomultiplier (Hamamatsu, Japan) operated in single-photon-counting mode. The detection spot was ~0.5 mm in diameter and hence encompassed $>10^8$ molecules.

Results and discussion

Following the introduction of the employed measurement technique, the discussion of results divides into three sections which deal with the systematic variation of different experimentally accessible parameters: the magnitude of the applied potentials, DC offsets of the substrate potential, and the concentration as well as valence of the salt added to the electrolyte solution.

Experimental methodology

The basic measurement principle which has been used throughout this work is depicted in Fig. 1. A low frequency (0.2 Hz), square wave potential modulation is applied to the gold electrodes which support the DNA layer under investigation. Simultaneously, the fluorescence emitted from dye labels attached to the DNAs' distal ends is monitored and found to be modulated with the same frequency as the electrical signal, yet phase-shifted by 180°. The origin of the observed fluorescence modulation can be explained in this way: the intrinsically negatively charged DNA is either repelled from the negatively charged, or attracted towards the positively charged electrode surface. Energy transfer from the optically excited dye labels to surface plasmons in the metal substrate suppresses their fluorescence emission as they approach the surface. Theoretical considerations treating the properties of oscillating dipoles above metal surfaces[16–18] show that the fluorescence quenching follows a power law dependence, $F \propto z^3$

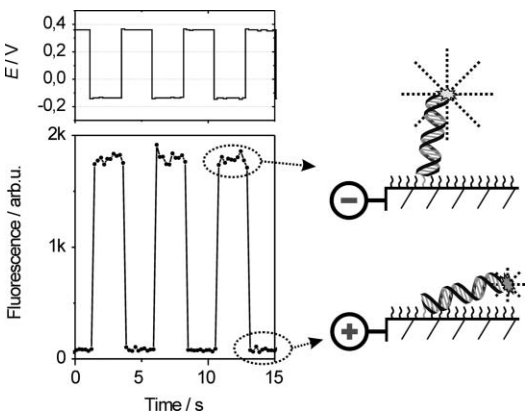

Fig. 1 Electrically switchable DNA layers. Left: Alternating potentials are applied to the gold substrate (*vs.* a Ag/AgCl reference electrode) while the fluorescence emission from the dye-labelled DNA layer is measured simultaneously. Right: the negatively charged DNA is repelled from negatively, or attracted to positively charged electrodes, respectively. The dashed rays indicate the intensity of the fluorescence emission, which is quenched if the dye approaches the metal surface.

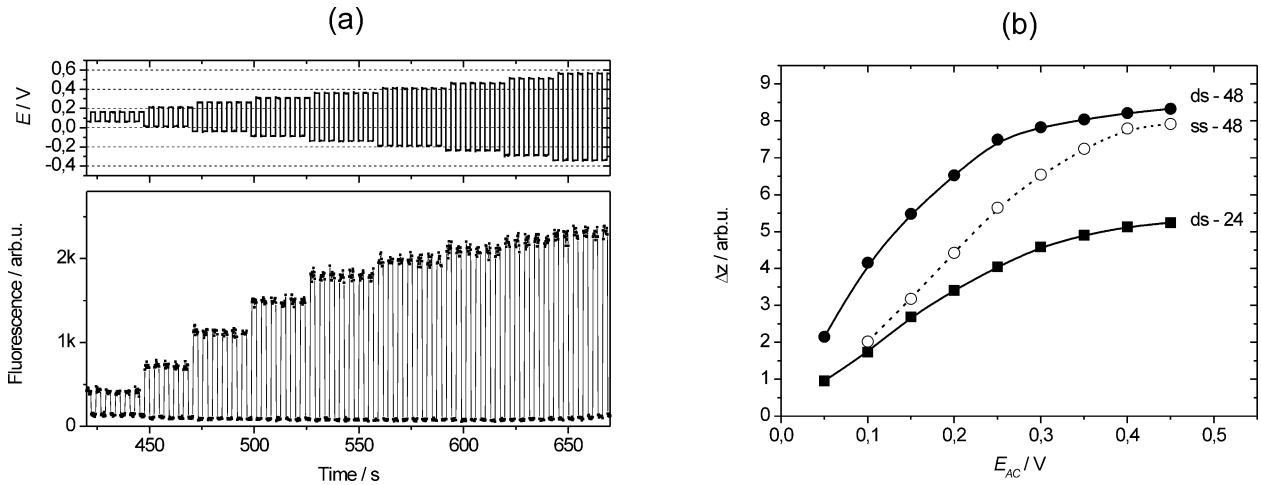

Fig. 2 (a) Electrically induced fluorescence modulation observed from a *ds*-48-bp DNA layer in 10 mM Tris buffer solution (electrode potential *E vs.* Ag/AgCl reference). (b) *z*-height modulation amplitude (evaluated from fluorescence measurements) as a function of AC amplitude. Lines are guides to the eye. The data have been normalized by the molecule surface densities of the samples, and differences in the fluorescence emission from *ss* and *ds*-DNA have been taken into account.§

(*F* being the emitted fluorescence, *z* being the normal distance of the emitter to the metal), in the range of *z*-values of interest.

This method allows the determination of the average height of the DNA layer in a contactless mode *in-situ* and in *real-time*.‡

Electric field strength

In the following, we elucidate the influence of the magnitude of applied electrode potentials on the DNA layer structure. Fig. 2(a) shows a representative switching response of a double stranded 48 mer DNA layer when gradually increasing the AC amplitude which is applied to the gold substrate. After increasing rapidly at first, the fluorescence modulation amplitude saturates for large electrical driving amplitudes. Evidently, the fluorescence is almost saturated to its minimal value from the beginning for attractive (positive) potentials, whereas in the repulsive (negative) regime the voltage must be more intensified in order to reach an equilibrium. This asymmetry arises from the particular choice of the DC offset which will be discussed later.

In accordance with the quenching argument elucidated above, the saturated fluorescence modulation amplitude can be attributed to a transformation of the layer structure between a condensed and extended state for attractive and repulsive electrode potentials, respectively. In these layer conformations, the DNA molecules are either predominantly 'lying' or 'standing' on the substrate.

We note that the range of potentials which can be applied to the gold electrodes without causing electrochemical degradation to the grafted DNA layers is limited to approximately the values shown in Fig. 2. For electrode bias more negative than app. −0.6 V (*vs.* Ag/AgCl), desorption of DNA molecules by virtue of strong electrostatic repulsion and reduction of the S–Au bond sets in;[19,20] for potentials more positive than +0.5 V we observe declining fluorescence emission from the layers, probably due to oxidation of the dye label.

In order to compare the manipulation efficiency for DNA molecules of different length and molecular conformation (namely, single and double stranded DNA), the average layer height has been estimated by deconvoluting the fluorescence data using the $F \propto z^3$ law and is shown in Fig. 2(b).

Molecular flexibility

A comparison of single and double stranded 48-bp DNA shows that the increase in the height modulation amplitude (Δz) with increasing AC voltage amplitudes sets in earlier and is steeper for *ds*-DNA (*cf.* Fig. 2(b)). For high electric field strengths, the single stranded trace approaches its double stranded counterpart.

We attribute the smoother rise in Δz to the different flexibility of the single stranded conformation. The distinct mechanical nature of the used single or double stranded oligonucleotides becomes apparent when contrasting their contour lengths, which is 16 nm in case of the *ds*-48-bp nucleotides, with their persistence lengths, which are 50 nm[21] for *ds*, but only 2–3 nm[22] for *ss*-DNA (the flexural persistence length defines the distance over which the direction along a polymer persists; correlations between orientations of two polymer segments fall off exponentially with this characteristic decay length). Evidently, the oligonucleotide length interpolates between these values and thus *ss*-oligonucleotides must be regarded as extremely flexible whereas *ds*-oligonucleotides are almost rigid rods.

These dissimilar mechanical properties have to be considered in conjunction with the strong electric field gradient that exists at the interface. When a charged surface is in contact with electrolyte, mobile ions in solution redistribute within the interface region and form a cloud of counterions, the electrochemical double layer (*cf.* Gouy–Chapman–Stern theory, see, for instance, ref. 12). Owing to this screening effect, the electric potential decays rapidly within short distances (typically a few nm), which conversely generates

‡ Owing to the low coverage of molecules on the surface, indications for mutual quenching of dye molecules within the layer have not been observed.

§ The oligonucleotides used (as obtained from IBA GmbH, Cy3 was NHS coupled) showed an enhancement of the Cy3-dye emission (factor 1.7) when hybridizing *ss*-DNA with strands of complementary sequence.

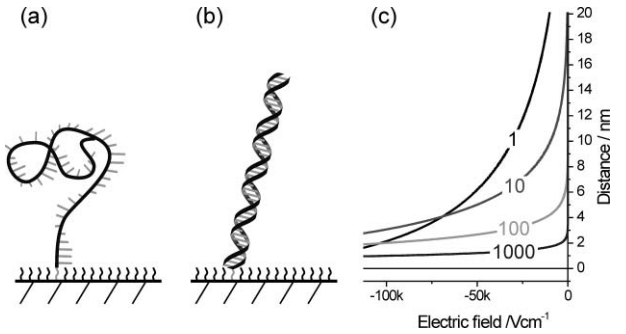

Fig. 3 Schematic structure of (a) *ss* and (b) *ds* 48 mer oligonucleotides on negatively charged surfaces. (c) Electric field within the Gouy–Chapman layer, calculated for different concentrations of monovalent salt (numbers denote the concentrations in mM) and an electrode potential of −0.1 V.

strong local electric fields. In Fig. 3, the gradient of the electric field calculated according to the Gouy–Chapman model is put side by side with schematic cartoons of *ss* and *ds* 48 mer DNA molecules, approximately drawn to scale. It shows that only the bottom-most segments of an end-tethered DNA molecule are exposed to high field strengths. For that reason, we suggest that the structures of *ss* and *ds*-oligonucleotides in localized (repulsive) fields differ as indicated in Fig. 3(a) and (b): Only the lower parts of the flexible *ss*-DNA are stabilized by the electric field, while the upper part of the molecule is significantly coiled up. Due to the intrinsic stiffness of *ds*-DNA, the electric torque exerted on a few bottom-most segments aligns the molecule's upper parts by leverage (this notion is supported by recent Brownian dynamics simulations, see reference 8).

Differences in the charge of *ss* and *ds*-DNA are not considered here, because both molecular conformations are expected to feature approximately the same *net* charge according to the theory of counterion condensation.[23]

Molecular contour length

Besides data for different molecular flexibility, Fig. 2(b) also compares results for oligonucleotides of different length, namely *ds*-24-bp and *ds*-48-bp DNA. Remarkably, the evaluated height modulations agree reasonably well with the expectation $\Delta z^{ds\text{-}48} \approx 2\Delta z^{ds\text{-}24}$. Slight discrepancies might be attributable to the minor relative stiffness (persistence-length divided by molecular-length) of the longer oligonucleotide.

It is particularly interesting that the shape of the 24 and 48-bp curves are very similar; in fact, when normalized to their maximum values, both curves almost coincide (not shown). We assign this to the fact that thermodynamics govern the alignment of DNA molecules on the surface: the average orientation of the molecules adjusts according to a balance of thermally induced disorder (Brownian motion) and electrically induced order (alignment within the electric field). Notably, 24 and 48-bp molecules are exposed to the same Brownian stimulus since the thermal energy of a particle does not depend on its size. For the reason that the electric field has such a short range, the strength of the electric interaction is practically the same for both DNA lengths, too. Consequently, the manipulation efficiency is largely independent of the DNA length.

DC bias and potential of zero charge

Earlier we argued that the DNA is expected to be repelled from, or attracted to, the gold substrate when alternating the surface charge. However, experimentally one usually defines the electrode potential with respect to an arbitrarily chosen reference electrode, which makes controlling the electrode charge a tricky issue. Obviously, it is important to know the potential which must be externally applied to the work electrode so that its surface charge vanishes. This value is generally termed the potential of zero charge (*pzc*). Intuitively, one would expect that the orientation of a charged molecule on a surface can be modulated most efficiently if the DC component of the driving voltage matches the *pzc*.

In order to test this assumption, we applied a constant AC modulation of small amplitude (50 mV) to 48 mer DNA layers while sweeping the DC component of the electrode bias from −0.3 to +0.4 V (*vs.* Ag/AgCl). The results are plotted in Fig. 4¶. For very positive DC bias (>0.2 V) the orientations of the DNA layers are not modulated by the AC component. Instead, the fluorescence intensity is found to nearly vanish during both repulsive and attractive periods indicating that the nucleic acids are lying on the surface at all times. When the DC offset is shifted negatively, the oligonucleotides lift off the surface during repulsive periods and gradually adopt more upright orientations. As E_{DC} becomes negative, the *ds*-DNA layer ceases to lie down completely during attractive periods (Fig. 4a and b). After crossing this intermediate regime, the saturation of the fluorescence during repulsive electrode potentials (F^{rep}) signifies that the strands are approaching a fully upright position. F^{attr} shows the same, yet delayed trend. In comparison to the double stranded layer, the 'lift-off' of *ss*-DNA for repulsive potentials is slightly shifted to negative bias, which is accompanied by a shift in the maximal fluorescence modulation, ΔF (Fig. 4c). Panels (b) and (c) in Fig. 4 also contain plots of the deconvoluted layer height (open symbols and dashed lines). At first inspection, the calculated *z*-values for very positive electrode bias may seem surprisingly high. However, estimating the orientation of the rod-like *ds*-48 bp DNA in that regime yields an average DNA–surface angle of approximately 10°; thus, the notion of 'lying' molecules seems justified.

The point of maximal layer height modulation, E_{DC}^{max}, corresponds to *pzc*-values reported for polycrystalline gold surfaces, *pzc* ≈ 0.0 V (*vs.* Ag/AgCl).[24,25] However, a comparison of the presented results with *pzc* values from the literature must be treated with care, because the *pzc* is known not only to depend on crystal orientations (for example, $pzc_{Au\langle 111\rangle} = +0.29$ V,[26] whereas $pzc_{Au\langle 210\rangle} = -0.17$ V[27]) but also on the chemical nature of the ions present in solution (different electrolyte compositions were used in references 24 and 25). In particular, the specific adsorption of Cl^- ions on gold[28] prohibits a determination of the *pzc* in Cl-containing electrolytes from impedance measurements; in the experiments shown in Fig. 4, the solution contained Cl-anions stemming from the buffer salt, Tris·Cl.

¶ Note that all investigations have been performed with DNA layers of low surface coverage in order to prevent lateral steric interactions within the layers. For layers with higher packing densities we observed curves which were significantly shifted towards positive E_{DC} compared to the data shown in Fig. 4.

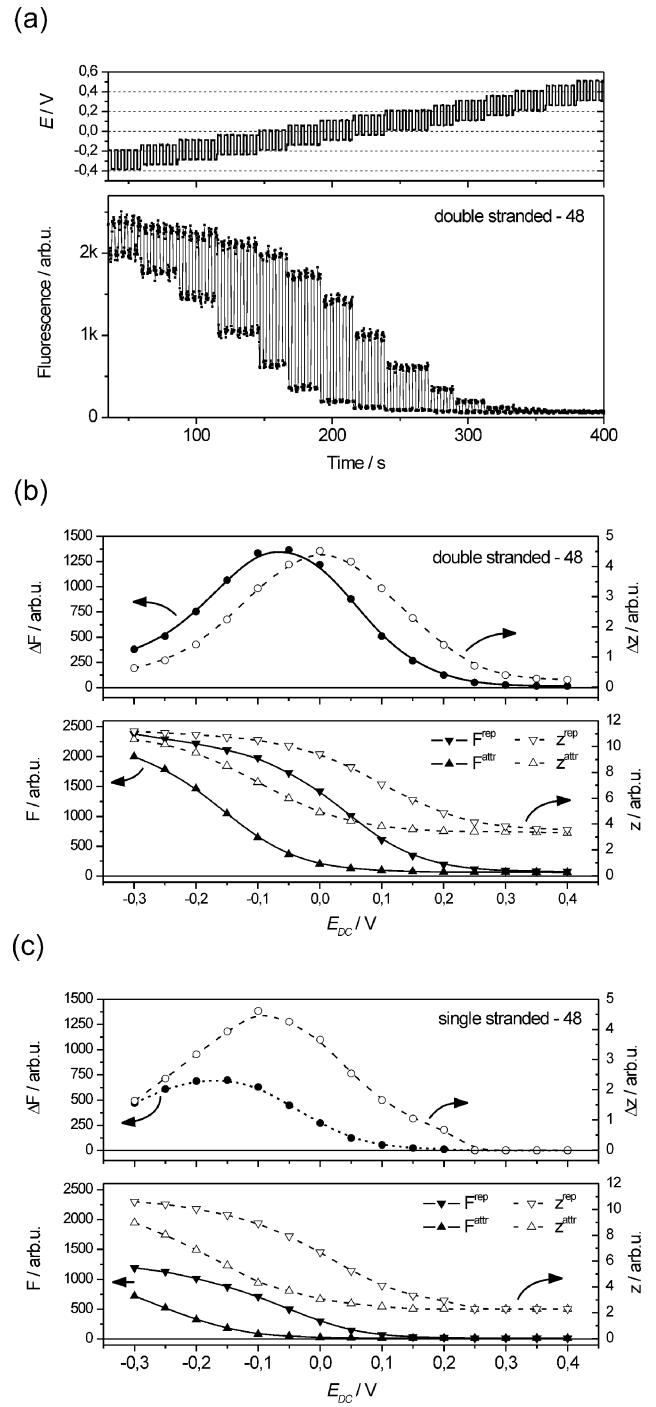

Fig. 4 (a): Fluorescence modulation observed from an electrically driven *ds*-48-bp DNA layer upon sweeping the DC electrode bias. (b) and (c): Analysed fluorescence (solid lines) and height (dashed lines) modulation as a function of DC bias for *ds* and *ss*-DNA layers. Note that the maxima of the height modulation Δz are shifted with respect to fluorescence data, owing to the non-linearity of the deconvolution $z \propto F^{1/3}$. Measurements were conducted in 10 mM Tris buffer, lines are guides to the eye.

An important result of Fig. 4 is that the modulation amplitude does not feature a sharp maximum but exhibits a broad distribution with respect to E_{DC}. This indicates that the substrate itself is characterized by a broad distribution of (local) *pzc*-values, which is expected for a polycrystalline surface.

Local field strength

At this point, we shall re-examine a peculiarity in the data of Fig. 2 which has not been discussed yet, namely the observation that AC amplitudes larger than 0.2 V actually result in more efficient DNA switching amplitudes. This is noteworthy, because it is not expected from the Gouy–Chapman–Stern model. According to GCS, the magnitude of the electric field at the DNA position, *i.e.*, a few nm from the surface, is not altered when increasing the electrode bias above ~0.2 V with respect to the *pzc*, because the additional voltage drops across the Stern layer (the first layer of counter-ions), while the diffuse Gouy–Chapman layer remains almost unaffected.

The broad maximum of the height modulation as a function of E_{DC} in Fig. 4(b) and (c), however, suggests the following interpretation: for a polycrystalline surface, the local variation in the *pzc* results in a variation of the local electric field above different crystal facets; consequently, DNA molecules attached to different facets are exposed to varying electrical interaction strengths. When increasing the magnitude of the electrode potential, the distribution of local *pzc* values superimposes to the externally applied voltage. Hence, in order to manipulate all DNA molecules on a macroscopic electrode with maximal efficiency, electrode potentials which are more negative than pzc_{min} −0.2 V or more positive than pzc_{max} +0.2 V must be applied to cause all DNA molecules to 'stand' or 'lie' on the surface, respectively. Here pzc_{min} and pzc_{max} denote the most negative and most positive local (microscopic) *pzc*-values which are present on the surface, respectively.

Electrolyte screening

The influence of a charged substrate on a grafted polyelectrolye layer is crucially determined by the characteristics of the medium which transduces the electric interactions. Earlier, we argued that the electrode potential is rapidly screened into solution by a cloud of redistributed ions; now, we will address this screening effect in more detail. As can be seen from Fig. 3(c), the Gouy–Chapman equation predicts that the electric field becomes more localized at the interface in electrolyte solutions of higher ionic strength. Thus, the range of (strong) electric interactions between the surface and the attached DNA can be simply tuned experimentally by adjusting the concentration and valence of the salt which is added to the electrolyte.

Fig. 5 shows such a DNA switching experiment, during which the salt concentration has been gradually increased while constantly monitoring the fluorescence modulation amplitude. Starting at 3 mM, $Tris^{+}\cdot Cl^{-}$ (also used as a buffer) was added until a concentration of 10 mM was reached; consecutively, salt concentrations above 10 mM were adjusted by adding NaCl or $MgCl_2$, respectively. For both salts we observe declining DNA modulation amplitudes (*cf.* Fig. 5a), yet strikingly, the signal decays more rapidly when adding $MgCl_2$ to the solution (which comprises divalent cations and twice as many anions).

Fig. 5(b) shows a plot of the same data *versus* a characteristic screening parameter, the Debye length l_D. Remarkably, the trends observed for the different salts exhibit almost perfect agreement now. For large l_D (low salt concentrations) we find nearly saturated, maximal switching amplitudes. However, when the Debye screening length falls below *ca.* 2 nm (a distance which roughly encloses

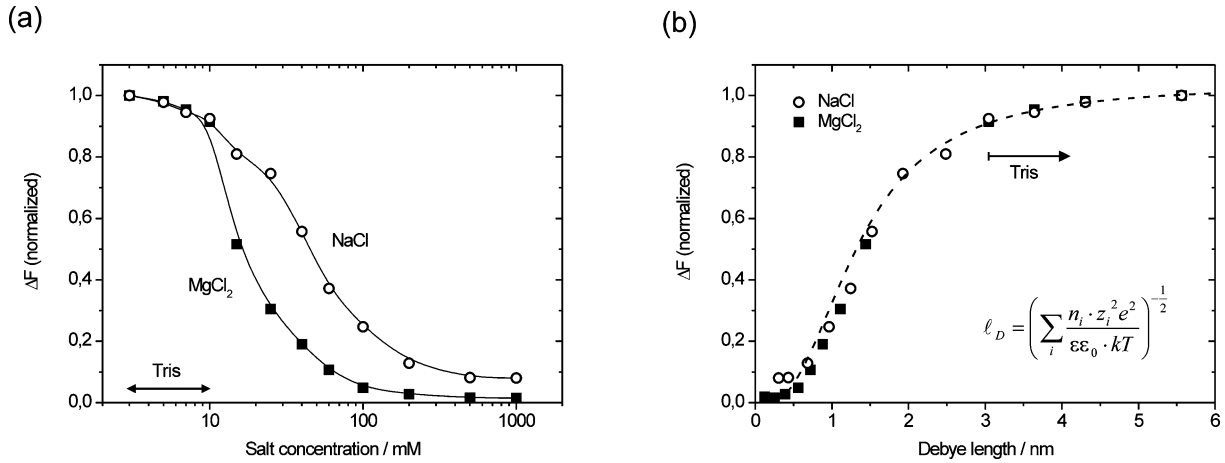

Fig. 5 (a) Fluorescence modulation amplitude as a function of electrolyte salt concentration (lines are guides to the eye); $E_{AC} = 0.2$ V, $E_{DC} = 0.2$ V *vs.* Ag/AgCl, $f = 0.2$ Hz, square wave. (b) Fluorescence modulation amplitude plotted *vs.* the Debye screening length l_D (inset: n_i = density of ion-species i, z_i = valence, e = elementary charge). The dashed line was calculated according to the charged-rod model described in the text.

the 6 bottom-most base pairs of a standing *ds*-DNA strand) the modulation amplitude drops rapidly until it essentially vanishes for very efficient screening, *i.e.*, short l_D.

These results show that electrolyte-mediated interaction of charged molecules and surfaces can adequately be described by basic screening arguments. Due to the strong electric field gradient, only the DNA segments closest to the surface are exposed to strong electric fields. As the extension of the Gouy–Chapman layer diminishes when increasing the salt concentration in solution, the electric interaction becomes too weak to efficiently align the DNA molecules on the surface.

Charged-rod model

In the previous sections we argued that the average DNA orientation adjusts according to a balance between entropy and electric alignment. Here, we elucidate this in some more detail by discussing a simple model system: a charged rod within the Gouy–Chapman potential. The rod, or more specifically, line-of-point-charges model should represent an acceptable approximation for *ds*-oligonucleotides, which feature a pronounced stiffness.

A sketch of the charged rod is depicted in the inset of Fig. 6. The rod-length is determined by the number of base pairs of the represented oligonucleotide (internucleotide spacing of *ds*-DNA = 0.34 nm). The rod is allowed to rotate freely around a pivot point, located at a distance $d = 1$ nm above the surface (corresponding to the length of the DNA linker as well as the thickness of the mercaptohexanol spacer layer). Electric interactions between the DNA and the surface are treated as follows: each base pair carries an effective charge of $q_{eff} = -0.24 \times 2e$ (e being the elementary charge), discretely localized along the rod. The intrinsic base pair charge $-2e$ is reduced according to the predictions of counterion condensation theory and assumed to be constant irrespective of the solution salt concentration.[23] The electric potential $\Phi(z)$ emanating from the electrode in the z-direction is given by the Gouy–Chapman expression ($T = 300$ K) and contains the Debye screening length, l_D (*cf.* the inset of Fig. 5b), and the surface potential, Φ_0, as parameters. We treat the DNA as a line of test charges within the undisturbed Gouy–Chapman potential;‖ the electrostatic energy, E, of the DNA-rod depends on its angle relative to the surface, θ, and is calculated by a summation over all point charges i [eqn (1)].

$$E = E_{\Phi_0, \ell_D}(\theta) = \sum_i q_{eff} \Phi(Z_i) \quad (1)$$

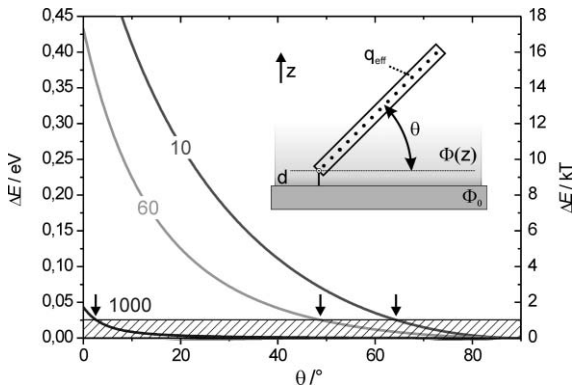

Fig. 6 Calculated electrostatic energy of a negatively charged rod (corresponding to *ds*-24-bp DNA) within the repulsive Gouy–Chapman potential above a negatively biased surface ($\Phi_0 = -0.2$ V). Concentrations of monovalent salt in solution are 10 mM ($l_D = 3.1$ nm), 60 mM ($l_D = 1.2$ nm), and 1000 mM ($l_D = 0.3$ nm).

Since θ is the rod's only degree of freedom, we are interested in the range of accessible energies with respect to θ. Choosing the energy of a standing rod as a reference, we consider ΔE ($= E(\theta) - E(\theta = 90°)$).

Fig. 6 shows ΔE calculated as a function of θ for different concentrations of monovalent salt in solution and a repulsive surface potential of -0.2 V. The rod length corresponds to a *ds*-24-bp DNA strand. It is instructive to scale the electric energy of the rod in units of the thermal energy kT, because it shows that

‖ Note that for large electrode potentials or solutions of high ionic strength, a Stern layer will develop at the surface; however, due to its small thickness, it is neglected here.

above some critical angle, kT prevails over the electric interaction; this regime is indicated by the hatched box in Fig. 6. For example, in the case of 10 mM salt concentration, the rod can be expected to be efficiently pushed away from the surface to angles larger than *ca.* 65°; subsequently, the rod orientation will be governed by stochastic motions. For a salt concentration of 1000 mM the critical angle is smaller than 5° due to the weak electric interaction. Hence, the orientation of the rod is largely unaffected by the electric field.

The average orientation of the rod can be obtained by employing Boltzmann statistics to account for the system entropy and electrical interactions.

$$\overline{\theta} = \frac{\sum \theta \cos\,\theta \exp\left\{-\frac{\Delta E_\theta}{kT}\right\}}{\sum \cos\theta \exp\left\{-\frac{\Delta E_\theta}{kT}\right\}} \qquad (2)$$

The summations are carried out over all possible zenith (out-of-surface-plane) angles. The factor $\cos\,\theta$ takes rotations around the azimuth (in-plane) angle into account, which are degenerate in energy. By evaluating eqn (2) for attractive and repulsive surface potentials the observable fluorescence modulation amplitude can be obtained††.

The dashed line in Fig. 5(b) has been computed for varying Debye lengths and alternating electrode bias of ±0.2 V. Two parameters were adjusted in order to fit the calculation to the experimental data; one of which is a trivial scaling constant (3.3×10^{-6}). The other, θ_{min}, restricts the evaluation of the sums in eqn (2) (*i.e.*, the summations were carried out for angles between $\theta_{min} = 35°$ and $\theta = 90°$) and bears physical relevance as it represents the minimal angle which can be adopted by DNA strands relative to the surface‡‡. Several reasons can limit the range of accessible angles: for instance, the packing density of the DNA layer can be too high; second, steric hindrance between the lowest segments of the DNA and the surface (or the mercaptohexanol spacer layer) might obstruct the lie-down process; third, the magnitude of the applied (positive) potentials might not be high enough to switch *all* the strands in the layer. The dominant mechanism may not be disclosed at this point, yet packing density effects seem unlikely as the measured average DNA surface coverage (3.3×10^{11} molecules cm^{-2}) is markedly below the expected onset of steric interactions. Even so, the appearance of a non-vanishing minimal angle is not very surprising recalling the data depicted in Fig. 4. Here we already found non-zero z-values for positive electrode potentials, which points to the fact that the molecules were not lying completely flat on the surface.

Considering the simplicity of the model and the few adjusted parameters the correspondence to the experiment seems quite satisfying and supports the discussion presented above. The DNA orientation adjusts according to a balance of thermally induced disorder and electrically induced order, the latter depending on the screening of electric fields by the electrolyte solution.

†† When calculating the average fluorescence, the factor $(l \times \sin\,\theta)^3$ enters the sum in the numerator, in order to take the fluorescence quenching into account (l is the DNA length).

‡‡ When setting $\theta_{min} = 0°$, the steepness of the calculated curve overestimates the experimental data.

Conclusions

We demonstrated that the structure (orientation) of oligonucleotides on surfaces can efficiently be manipulated by applying moderate bias potentials to the substrates supporting the monolayers. The obtained results indicate that the switchability of DNA layers depends on the (laterally varying) local field strength above the surface which is influenced by the externally applied electrode potential in conjunction with the distribution of local potential of zero charge values. This is of particular importance when dealing with polycrystalline metal surfaces, which are most relevant to applications.

Further, it is essential to consider the electrolyte which mediates electric interactions between the surface and the tethered polyelectrolyte. Due to efficient screening in solutions of high ionic strength, the electric field decays so rapidly into solution that the interaction is too weak to manipulate the DNA orientation, which is then governed by stochastic thermal motions.

Experiments with *ss* and *ds*-DNA show that their distinct molecular conformation (*i.e.*, flexibility) significantly affects the structure of the oligonucleotides at the surface; these findings are expected to be generally valid for charged, linear macromolecules which are exposed to high field gradients at interfaces.

Acknowledgements

We are most grateful to Yoshitaka Yamaguchi for the wafer preparation. This work was financially supported by the Fujitsu Laboratories of Europe and in part by the DFG *via* SFB563. One of the authors (M.T.) gratefully acknowledges funding by the BMBF under grant 03N8713 (Junior Research Group "Nanotechnology").

References

1 M. J. Tarlov and A. B. Steel, in *Biomolecular Films*, ed. J. F. Rusling, Marcel Dekker Inc., New York, 2003, vol. 111, pp. 545–608.
2 M. J. Heller, *Annu. Rev. Biomed. Eng.*, 2002, **4**, 129–153.
3 R. Levicky, T. M. Herne, M. J. Tarlov and S. K. Satija, *J. Am. Chem. Soc.*, 1998, **120**, 9787–9792.
4 D. Y. Petrovykh, H. Kimura-Suda, L. J. Whitman and M. J. Tarlov, *J. Am. Chem. Soc.*, 2003, **125**, 5219–5226.
5 R. Georgiadis, K. P. Peterlinz and A. W. Peterson, *J. Am. Chem. Soc.*, 2000, **122**, 3166–3173.
6 S. O. Kelley, J. K. Barton, N. M. Jackson, L. D. McPherson, A. B. Potter, E. M. Spain, M. J. Allen and M. G. Hill, *Langmuir*, 1998, **14**, 6781–6784.
7 U. Rant, K. Arinaga, S. Fujita, N. Yokoyama, G. Abstreiter and M. Tornow, *Nano Lett.*, 2004, **4**, 2441–2445.
8 U. Rant, K. Arinaga, M. Tornow, Y. W. Kim, R. R. Netz, S. Fujita, N. Yokoyama and G. Abstreiter, *Biophys. J.*, 2006, **90**, 3666–3671.
9 Z.-L. Zhang, D.-W. Pang and R.-Y. Zhang, *Bioconjugate Chem.*, 2002, **13**, 104–109.
10 H. Wackerbarth, M. Grubb, J. Zhang, A. G. Hansen and J. Ulstrup, *Angew. Chem., Int. Ed.*, 2004, **43**, 198–203.
11 E. Wierzbinski, J. Arndt, W. Hammond and K. Slowinski, *Langmuir*, 2006, **22**, 2426–2429.
12 A. J. Bard and L. R. Faulkner, *Electrochemical Methods*, Wiley & Sons, New York, 2nd edn., 2000.
13 T. M. Herne and M. J. Tarlov, *J. Am. Chem. Soc.*, 1997, **119**, 8916–8920.
14 U. Rant, K. Arinaga, S. Fujita, N. Yokoyama, G. Abstreiter and M. Tornow, *Langmuir*, 2004, **20**, 10086–10092.
15 A. B. Steel, T. M. Herne and M. J. Tarlov, *Anal. Chem.*, 1998, **70**, 4670–4677.
16 R. R. Chance, A. Prock and R. Silbey, *Adv. Chem. Phys.*, 1978, **37**, 1–65.

17 W. L. Barnes, *J. Mod. Opt.*, 1998, **45**, 661–699.
18 B. N. J. Persson, *J. Phys. C: Solid State Phys.*, 1978, **11**, 4251–4269.
19 J. Wang, G. Rivas, M. A. Jiang and X. J. Zhang, *Langmuir*, 1999, **15**, 6541–6545.
20 S. Takeishi, U. Rant, T. Fujiwara, K. Buchholz, T. Usuki, K. Arinaga, K. Takemoto, Y. Yamaguchi, M. Tornow, S. Fujita, G. Abstreiter and N. Yokoyama, *J. Chem. Phys.*, 2004, **120**, 5501–5504.
21 S. B. Smith, L. Finzi and C. Bustamante, *Science*, 1992, **258**, 1122–1126.
22 B. Tinland, A. Pluen, J. Sturm and G. Weill, *Macromolecules*, 1997, **30**, 5763–5765.
23 G. S. Manning, *Q. Rev. Biophys.*, 1978, **2**, 179–246.
24 D. I. Leikis, K. V. Rybalka, E. S. Sevastyanov and A. N. Frumkin, *J. Electroanal. Chem.*, 1973, **46**, 161–169.
25 J. Bockris, S. D. Argade and E. Gileadi, *Electrochim. Acta*, 1969, **14**, 1259–1283.
26 A. Hamelin, T. Vitanov, E. S. Sevastyanov and A. Popov, *J. Electroanal. Chem.*, 1983, **145**, 225–264.
27 J. Lecoeour, J. Andro and R. Parsons, *Surf. Sci.*, 1982, **114**, 320.
28 J. Wang, A. J. Davenport, H. S. Isaacs and B. M. Ocko, *Science*, 1992, **255**, 1416–1418.